

# Fast Recoating Methods for the Projection-based Stereolithography Process in Micro- and Macro-Scales

Yayue Pan, Yong Chen\*, Chi Zhou

Daniel J. Epstein Department of Industrial and Systems Engineering  
University of Southern California  
Los Angeles, CA 90089, U.S.A.

\*Author of correspondence, Phone: (213) 740-7829, Fax: (213) 740-1120, Email: [yongchen@usc.edu](mailto:yongchen@usc.edu)

## ABSTRACT

The purpose of this paper is to present a recoating method for the development of a direct digital manufacturing (DDM) process that can be an order of magnitude faster than other currently available DDM processes. In the mask-image-projection-based Stereolithography (MIP-SL) process, projection light controlled by a Digital Micromirror Device (DMD) can quickly cure liquid photopolymer resin in a whole area; a fast recoating method is required for achieving truly high-speed fabrication. We investigate the bottom-up projection system in the MIP-SL process. For the macro-scale MIP-SL process, a two-way linear motion approach has been developed for the quick spreading of liquid resin into uniform thin layers. In comparison, a direct pull-up motion can be used in the micro-scale MIP-SL process. The system design and related settings for achieving a fabrication speed of a few seconds per layer are presented. Additionally, the hardware, software, and material setups for fabricating three-dimensional (3D) digital models are presented. Experimental studies using the developed testbed have been performed to verify the effectiveness and efficiency of the presented fast MIP-SL process.

## KEYWORDS

Additive manufacturing, high-speed fabrication, fast recoating, stereolithography.

## 1 INTRODUCTION

Layer-based *Additive Manufacturing* (AM) processes such as *Stereolithography Apparatus* (SLA) can fabricate parts directly from Computer-aided Design (CAD) models without part-specific tooling or fixtures. As a direct manufacturing approach, AM processes can cost-effectively fabricate truly complex three-dimensional (3D) shapes that were previously impossible. Unlike traditional prototyping approaches that take days, AM-based rapid prototyping can build physical objects in hours. Due to such time and cost benefits, AM processes have been widely adopted in the product development process for building prototypes of a design.

Although the speed of AM systems has significantly increased over the years, the building process of a moderate sized 3D model is typically measured in hours. In a recent NSF workshop on developing *the roadmap for AM* [1], the development of AM machines with higher throughput was identified to be critical for future rapid manufacturing requirements. Future high-speed AM systems require new approaches, evolving from point-processing or line-processing methods such as a laser or an extruding nozzle, to area-processing or volume-processing methods.

In this research, we investigate the building speed of an area-processing approach that is based on a *Digital Micromirror Device* (DMD). A DMD is a microelectromechanical system (MEMS) device that enables one to simultaneously control  $\sim 1$  million small mirrors that turn on or off a *pixel* at over 5 KHz. Using this technology, a light projection device can project a dynamically defined mask image onto a resin surface to selectively cure liquid resin into layers of the object. Consequently, the related AM process, *Mask-Image-Projection-based Stereolithography* (MIP-SL), can be much faster than the laser-based SLA process by simultaneously forming the shape of a whole layer. An illustration of the MIP-SL process is shown in Figure 1. In the MIP-SL process, a 3D CAD model of an object is first sliced by a set

of horizontal planes. Each thin slice is converted into a two-dimensional (2D) mask image. The mask image is then sent to the DMD and projected onto a photocurable resin surface to form the shape of the related layer. By repeating the process, 3D objects can be fabricated on a layer-by-layer basis.

### 1.1 Building Speed Limitation of the MIP-SL Process

In the MIP-SL process, the building time of each layer consists of spreading liquid resin into a uniform thin layer and curing the formed liquid layer into a solid layer. Compared to a laser beam that is used in the SLA process, the DMD used in the MIP-SLA process can dramatically decrease the curing time of a layer. Hence, the bottleneck for achieving a fast building speed is the spreading of liquid resin into uniform thin layers, which is the focus of the paper.

Research systems (e.g. [2-8]) and commercial systems (e.g. [9, 10]) have been developed before based on the mask image projection approach. Most of the developed systems are based on the top-down projection as shown in Figure 1. Suppose  $d_{LT}$  is the layer thickness. After a previous layer has been cured, the platform in such a system usually moves down a certain distance  $d$  and then up by  $d-d_{LT}$  in order to spread liquid resin into a uniform thin layer. In addition to the Z movement, a recoating process is usually required to sweep through the platform such that the top surface can be flattened. For resin with low viscosity, a deep-dip recoating approach has also been developed to replace the surface sweeping approach. After the up and down movements in the Z axis, a sufficient waiting time is required for the liquid resin to settle down into a flat surface. However, such recoating methods are time consuming, which limits the building speed of the MIP-SL process. Consequently, the building time of such MIP-SL systems is still measured in hours.

### 1.2 Contributions

To address the building speed limitation of the MIP-SL process, we present recoating approaches for quickly spreading liquid resin into uniform thin layers. For macro-scale parts, our approach is based on a two-way movement design in a bottom-up projection system. We addressed the related challenge of large attaching forces in the bottom-up projection system. By optimizing the process settings, we illustrate that the preparation of a uniform thin layer can be done within seconds. Consequently, the developed fast MIP-SL process can build moderate sized parts in minutes instead of hours.

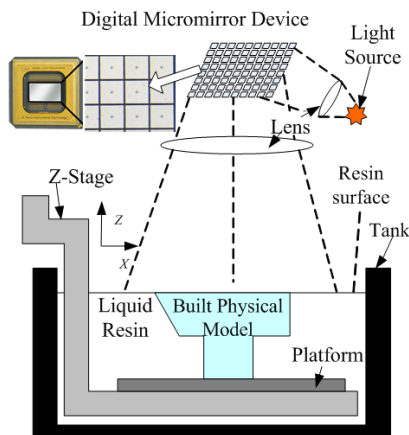


**Figure 1: An illustration of the MIP-SL process.**

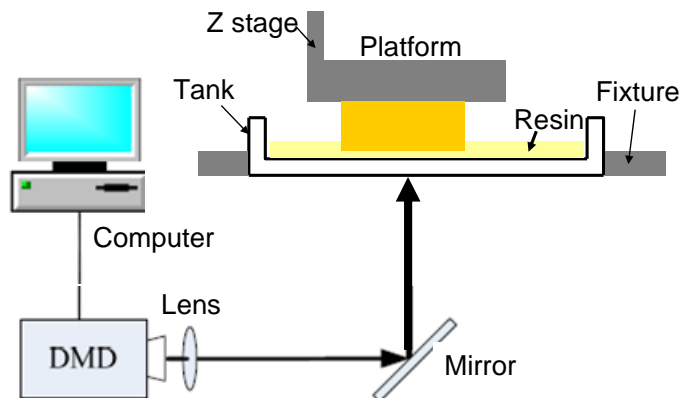


**Figure 2: An illustration of the bottom-up projection system.**

## 2 BOTTOM-UP PROJECTION BASED MIP-SL SYSTEM

In addition to the top-down projection approach as shown in Figure 1, another projection approach used in the MIP-SL process is the bottom-up projection as shown in Figure 2. That is, the mask image is projected onto the bottom of a transparent tank. After a layer is cured at the bottom of the built part, the platform is moved up and then down to form a small gap with the bottom surface of the resin tank. A uniform thin layer can be achieved after the formed gap is filled with liquid resin.

## 2.1 Advantages of the Bottom-up Projection System

A bottom-up projection based system has several advantages over a top-down projection based system. (1) The container depth is independent of the part height. Thus a shallow vat can be used to reduce the required volume of the liquid resin. During the building process liquid resin can be added by a pump when needed. (2) Recoating is achieved by constraining liquid resin between the previously cured layers and the resin tank. Hence no additional sweeping is needed for flattening the resin surface. (3) Much smaller layer thickness can be achieved since the gap size is only determined by the Z stage resolution regardless of the fluid properties of liquid resin. (4) The curing of liquid resin is sealed from the oxygen-rich environment. By eliminating the oxygen inhibition effect, the liquid photopolymer resin can be cured faster.

## 2.2 Challenges of the Bottom-up Projection System

Despite the advantages, the bottom-up projection based system has not been widely used in the SLA and MIP-SL processes. A main reason is that the separation of the cured part from the tank surface is difficult. That is, in the bottom-up projection based MIP-SL process, a cured layer is sandwiched between the previous layer and the resin vat. The solidified material may adhere strongly to the corresponding rigid or semi-rigid transparent solidification substrate, causing the object to break or deform when the build platform moves up from the vat during the building process.

One approach to prevent the detachment of a cured layer from the built part is to increase its exposure such that the cured layer can strongly bond to the previous layers. However, such over-curing will also lead to poor surface quality and inaccurate dimensions. Another approach to address the problem is to apply a certain type of coating on the resin vat to reduce the attachment force of a cured layer. Suitable coatings, including Teflon and silicone films, can help the separation of the part from the vat [11, 12]. A coated Teflon glass has also been used in the machines of Denken [13] and EnvisionTec [9]. However, even with the intermediate material, the separation force can still be large. Huang and Jiang [12] investigated the attachment force for the coating of an elastic silicone film. Based on a developed on-line force monitoring system, test results indicate that the pulling force increases linearly with the size of the working area. Experiments indicate that, for a square of 60×60mm, the pulling force to separate the part from the film is greater than 60 N. Such a large attachment force between the cured layer and the vat is a key challenge that needs to be addressed in the bottom-up projection based MIP-SL process.

To reduce the large attachment force, another approach developed by EnvisionTec in its Perfactory Systems [9] is to incorporate additional mechanisms that add tilting motions in the part separation. That is, during the separation, one side of the platform can be moved up slowly before the other side. In this way, instead of the pulling-up, the part can be peeled off from the vat surface. Hence the detaching force would be significantly reduced. However, such additional tilting motion will also reduce the building speed of the MIP-SL process.

We address the large separation force and the related speed problem for large area parts by developing a two-way movement method. For the purpose of easy sliding between the built part and the resin tank, we use another type of coating material, Polydimethylsiloxane (PDMS, Sylgard 184, Dow Corning). The coating selection is based on the ability of PDMS in inhibiting free-radical polymerization near its surface, as shown by Dendukuri *et al* [14]. In their research, it was identified that a very thin oxygen-aided inhibition layer (~2.5 μm) is formed that can prevent the cured layer from attaching to the PDMS film. Thus cured layers can easily slide on the PDMS film. Based on the approach, a fast MIP-SL process has been developed that can build a CAD model in minutes.

The remainder of the paper is organized as follows. Part separation forces are analyzed in Section 3. A two-way movement approach to reduce the part separation force is presented in Section 4. Physical experiments on separation forces based on the PDMS film are presented in Section 5. The process settings and the related building time analysis are presented in Section 6. The experimental setup for performing physical experiments is discussed in Section 7. The experimental results of multiple test cases are presented in Section 8. Finally, conclusions with future work are given in Section 9.

### 3 SEPARATION FORCES OF THE BOTTOM-UP PROJECTION SYSTEM

A simple and intuitive approach for separating cured parts from a film is to directly move the platform up a certain distance  $d$  and then down by  $d-d_{LT}$  where  $d_{LT}$  is the layer thickness. Another approach is to move the cured parts horizontally by a certain distance  $D$ . The dominant forces that exist in such two approaches are analyzed and compared as follows.

#### 3.1 Separation Force in the Up-Down Movement

As shown in Figure 3a, when the platform is moving up, a small gap is formed between the cured part and the film. The resin flowing into the gap is determined by parameters such as the gap  $h$ , the surface area, the resin viscosity, and film surface tension. The pulling-up force is a combination of the viscosity and pressure difference that can be expressed as:

$$F_z = F_v + F_{Pc} + F_{Pd} = \int (\mu \frac{\partial v}{\partial x}) dz + \int \Delta P_c dh + \int \Delta P_d dx, \quad (1)$$

where  $\mu$  is the dynamic viscosity coefficient,  $\Delta p_c$  is the capillary pressure drop across the free surface, and  $\Delta p_d$  is the pressure difference between the inlet and the outlet.

The capillary pressure drop across the free surface is given by Laplace-Young equation:

$$\Delta p_c = \frac{2\sigma \cos \theta}{h}, \quad (2)$$

where the gap distance is  $h$ ,  $\theta$  is the wetting angle, and  $\sigma$  is the surface tension.

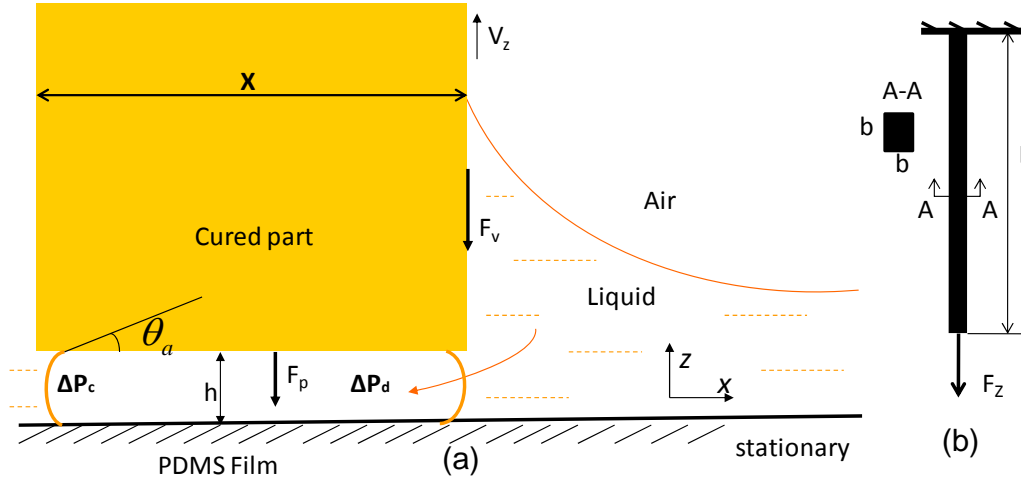


**Figure 3: An illustration of separation forces during the moving-up process.**

For the Newton flow in the system, the momentum equation can be written as:

$$\rho \frac{D\vec{v}}{Dt} = \vec{F} - \nabla p + \nabla \cdot \tilde{\tau}; \quad (3)$$

where  $\rho$ ,  $\vec{v}$ ,  $\vec{F}$ ,  $\nabla p$  and  $\tilde{\tau}$  are density, velocity, body forces and stress tensor, respectively.

To simplify the problem, we assume that: (i) the problem can be considered as two dimensional and symmetric; (ii) both film and cured surfaces are flat; (iii) the temperature fluctuation during the building process can be omitted; (iv) the tank is big enough such that the flow in the  $X$  direction can be considered as infinity; (v) the film can be considered as a fixed bottom wall. Hence the equation [3] can be rewritten in the  $X$  direction as:

$$\rho \left( \frac{\partial v_x}{\partial t} + v_x \frac{\partial v_x}{\partial x} + v_y \frac{\partial v_x}{\partial y} + v_z \frac{\partial v_x}{\partial z} \right) = - \frac{\partial p}{\partial x} + \mu \left( \frac{\partial^2 v_x}{\partial x^2} + \frac{\partial^2 v_x}{\partial y^2} + \frac{\partial^2 v_x}{\partial z^2} \right) + \rho g \quad (4)$$

Based on the fully developed and time independent flow assumptions,  $\frac{\partial v}{\partial t} = 0$  and  $\frac{\partial v_x}{\partial y} = \frac{\partial v_x}{\partial x} = 0$ . Therefore the Navier-Stokes Equation (4) can be modified as:

$$-\frac{\partial p}{\partial x} + \mu \frac{\partial^2 v_x}{\partial z^2} = \rho \frac{\partial v_x}{\partial t} = 0 \quad (5)$$

Based on the boundary condition  $v_x|_{y=h/2} = v_x|_{y=-h/2} = 0$ , the velocity of the flow front is:

$$\frac{dx}{dt} = u = \frac{1}{h} \int_{-h/2}^{h/2} v_x dz; \quad (6)$$

By combining Equations (5) and (6), we know:

$$\frac{dp}{dx} = \mu \frac{\partial^2 v_x}{\partial z^2} = \frac{12\mu}{h^2} \cdot \frac{dx}{dt}; \quad (7)$$

The pressure difference  $\Delta p_d$  is a function of the surface size:  $\Delta p_d \propto X$ .

As shown in the equations, the pulling-up forces  $F_v$  and  $F_{Pc}$  only relate to the length of the surface boundary; while  $F_{Pd}$  is determined by the size of surface area. In addition,  $F_{Pd} \propto A^n, n > 1$ . When the area  $A$  is relatively large,  $F_{Pd}$  is dominant in  $F_z$ . Hence,  $F_z \approx F_{Pd} \propto A^n, n > 1$ .

### Maximum Separation Force Before Breaking:

In the up-down moving process, the main separation force is in the  $Z$  direction. As shown in Figure 3b, the maximum separation force that can be added to the cured part is:  $F_{Max-z} = \sigma_t \times b^2 = \sigma_t \times A$ , where  $\sigma_t$  is the tensile strength of the material and  $b$  is the beam cross section size. That is, the maximum separation force before breaking follows:  $F_{Max-z} \propto A$ .

### 3.2 Separation Force in the Horizontal Movement

As mentioned before, there is a very thin oxygen-aided inhibition layer formed near the PDMS film. When sliding the cured part in the  $X$  direction, liquid resin will fill in the gap. As shown in Figure 4a, the main separation force during the sliding process is the shearing force related to the resin viscosity. That is,

$$F_x \approx F_v = \int \left( \mu \frac{\partial v}{\partial z} \right) dx. \quad (10)$$

Hence,  $F_x \propto A$ .

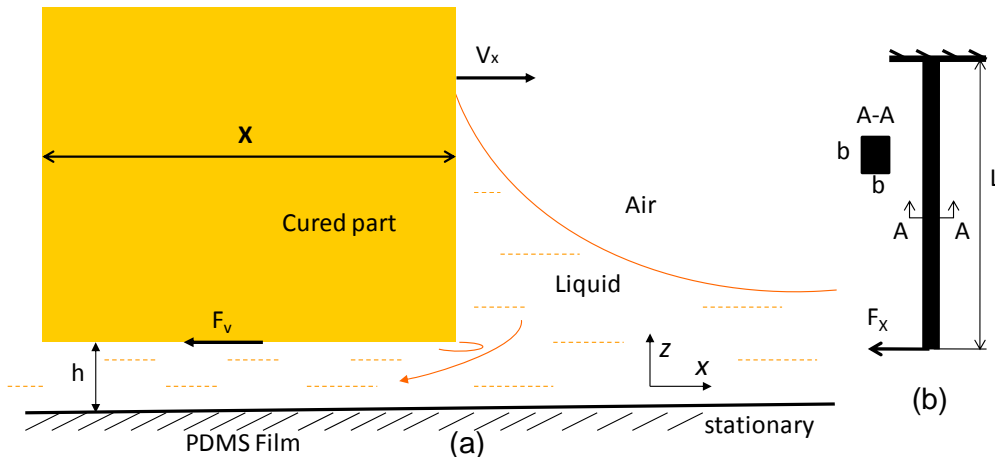


Figure 4: An illustration of the separation force during the sliding process.

### **Maximum Separation Force Before Breaking:**

As shown in Figure 4b, the maximum bending force allowed for a beam during the sliding process is:

$$F_B = \frac{\sigma_b \times b^3}{6L},$$

where  $\sigma_b$  is the flexural strength of the material,  $b$  is the beam cross section size, and  $L$  is the length of the beam. That is, the maximum separation force before breaking follows:  $F_{Max\_x} \propto A^{3/2}$ . (12)

### **3.3 Separation Force Comparison of the Two Movements**

As shown in Equations (8), (9), (11) and (12), the separation force and the maximum allowed forces in the Z and X directions have different relationships with the surface area.

- (a)  $F_z \propto A^n, n > 1$  and  $F_{Max\_z} \propto A$  when the cured part is moved in the Z direction;
- (b)  $F_x \propto A$  and  $F_{Max\_x} \propto A^{3/2}$  when the cured part slides in the X direction.

Accordingly, we know:

- (1) For an increasing part size  $A$ , the separation force  $F_z$  increases much faster than the maximally allowed force  $F_{Max\_z}$ . In comparison, the maximally allowed force  $F_{Max\_x}$  increases much faster than the separation force  $F_x$ . Consequently, for a large object size, it is desired to use the sliding movement in the X direction.
- (2) For a decreasing part size  $A$ , the maximally allowed force  $F_{Max\_x}$  decreases much faster than the separation force  $F_x$ . In comparison, the separation force  $F_z$  decreases much faster than the maximally allowed force  $F_{Max\_z}$ . Consequently, for a small object size, it is desired to use the up-down movement in the Z direction.

Therefore, a new recoating method that is based on the sliding movement in the X direction is needed for the macro-scale MIP-SL process. In contrast, the traditional resin recoating approach based on the up-down movement can be used for the micro-scale MIP-SL process. In the following sections, we will mainly discuss the new recoating method developed for the macro-scale MIP-SL process.

## **4 TWO-WAY MOVEMENT DESIGN FOR THE FAST MACRO-SCALE MIP-SL PROCESS**

The experiment results indicate that the suction force between the cured layer and the PDMS film is large during the pulling-up process. Such a large force on the cured layer may cause the building process to fail if the bonding force between the current layer and previous layers is smaller than the suction force. In addition, after building multiple layers, such forces on the PDMS film may lead to cracks in the film due to material fatigue caused by the cyclic loading.

Based on the PDMS film, we presented a two-channel design for the multi-material MIP-SL process [15]. However, such an approach, mainly designed for switching tanks, is not suitable for the fast building process. In the two-channel design, the building of each layer requires a full cyclic motion including both moving the platform up and down in the Z axis, and moving the tank back and forth in the X axis. Such motions will slow down the building process. To facilitate a high-speed MIP-SL process based on the bottom-up projection, a novel two-way movement design is developed, which requires much less motions than the two-channel design.

An illustration of the fast MIP-SL process based on the two-way movement design is shown in Figure 5. In our method, a transparent PDMS film is first applied on the bottom surface of a glass vat.

(1) After a mask image is exposed to cure a layer, the platform is moved up in the Z axis for one layer thickness (e.g. 50  $\mu\text{m}$ ). Accordingly, the regions of the PDMS film related to the shape of the cured layer will be pulled up by the suction force. However, the force is small due to the super elasticity of the PDMS film. Note that there is no liquid resin between the cured layer and the PDMS film at this moment.

(2) The tank is moved along the X axis for a certain distance  $\Delta x$ . A good property of the PDMS film is that a very thin oxygen-aided inhibition layer ( $\sim 2.5 \mu\text{m}$ ) is formed near the PDMS film that can provide a non-polymerized lubricating layer for easy sliding [14]. If the moving distance is sufficiently large (e.g.

larger than the extent size of the cured layer in the X axis), the elastic deformation of the pulled-up PDMS film will be released by such a sliding movement. Hence, at the end of the X movement, liquid resin will be filled in the small gap between the cured layer and the PDMS film.

(3) The mask image of a new layer can now be projected at the bottom surface to cure the next layer. These three steps can then be repeated by moving the tank in an opposite direction. Note that, to achieve the motion in the X direction, we only move the tank and the related frame. There is no relative motion between the platform and the projection device. Hence the XY accuracy of the MIP-SL system will not be affected by the X translations.

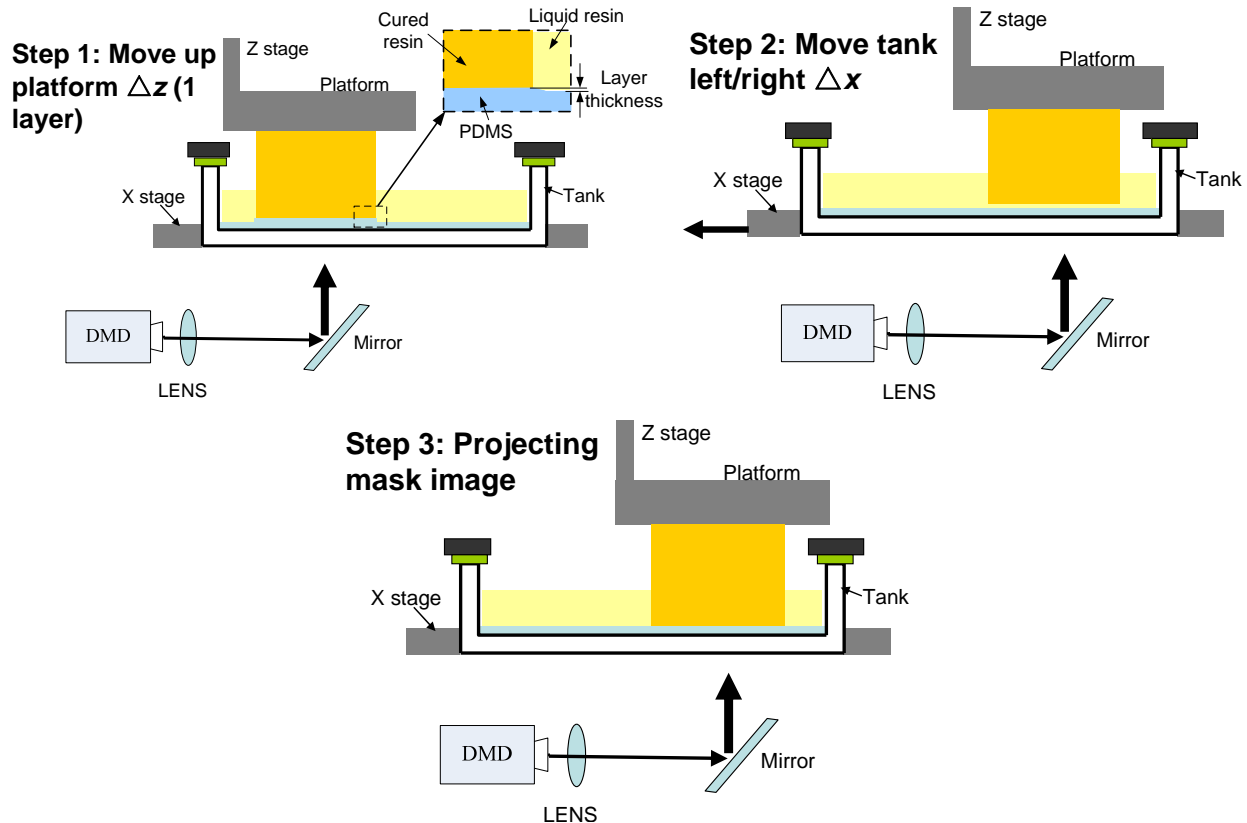


Figure 5: The MIP-SL process based on the two-way movement design with PDMS.

## 5 PART SEPARATION EXPERIMENTS BASED ON PDMS

Physical experiments on the separation forces have been presented. As shown in the test results, the two-way movement design can effectively reduce the large separation force while achieving a fast building speed at the same time.

### 5.1 Separation Force Study based on the Up-down Movement

We studied the part separation force of a cured layer from a coated PDMS glass based on moving the platform up a certain distance  $d$ . Since one layer thickness is usually very small (50-200  $\mu\text{m}$ ),  $d$  is usually much larger in order for the resin to fully fill the gap (e.g. 5mm). In our tests, the PDMS film thickness is set at 1mm. A set of physical experiments have been designed and performed to understand the separation force based on such up-down movement.

Figure 6a shows the setup for measuring the pulling-up force. Two FlexiForce sensors (Tekscan, South Boston, MA) with a range of 0-25 lbs are sandwiched between the fixture and the vat. The two sensors are connected to a microcontroller, which can sample and record the sensors' readouts at over 3KHz. Since the vat is free at the bottom and the side, and only fixed at the top, the pulling force by the part will be transferred to the sensors when the platform rises. In the experiments, we first use a given

mask image to build a certain number of layers (e.g. 25 layers). The layer thickness is set at 0.2mm. We then begin to record the separation force in the building process of the next few layers. For each layer, after the designed mask image has been exposed for a certain time, the platform is raised up slowly at 0.6mm/sec for 5mm and the related readouts of the sensors are then recorded.

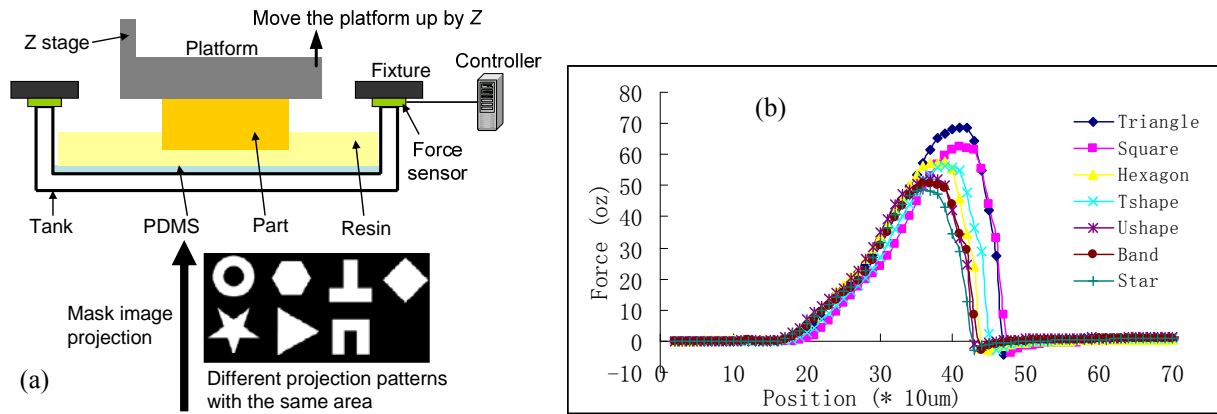


**Figure 6: Separation force study: (a) experimental setup for studying separation forces in the MIP-SL process; and (b) pulling-up forces of a cured layer for  $T=0.5$  sec, Area = 625 mm<sup>2</sup>.**

In our study, we considered three factors that may affect the separation force including (1) exposure time, (2) image area, and (3) image shape. To understand the effects of these factors, designed experiments were conducted. Seven projection patterns were used for testing the effect of image shape. They are shown in Figure 3, which include circle band, hexagon, t-shape, square, star-shape, triangle, and u-shape. For comparison, all the projection patterns have the same area in the tests. The separation forces of a cured layer were measured based on each of the seven projection patterns. Figure 6b shows the measured separation forces of a sensor for different test cases. The horizontal axis indicates the distance in the Z direction (in the unit of 10  $\mu\text{m}$ ), and the vertical axis indicates the measured pulling force (in ounces). The results of more test cases are shown in Figure 7.

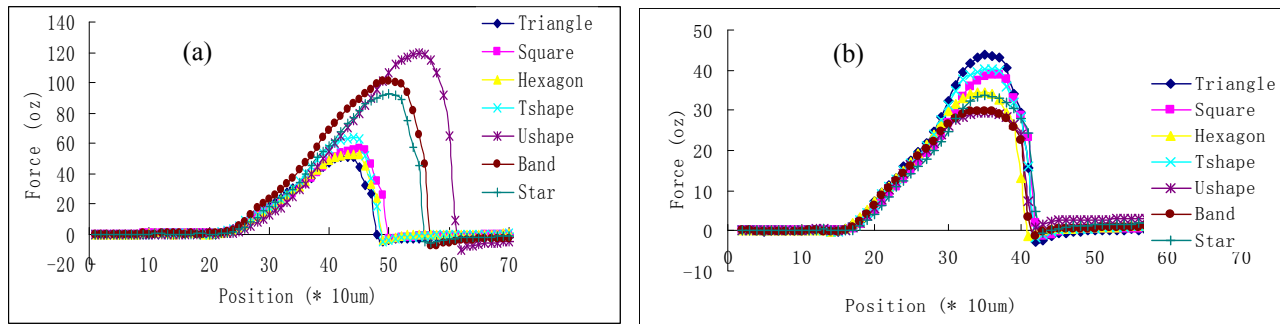


**Figure 7: Pulling-up forces of a cured layer from a PDMS film in different settings: (a)  $T=1$ sec, Area = 625 mm<sup>2</sup>; and (b)  $T=1$ sec and Area = 156 mm<sup>2</sup>.**

It can be observed from the experimental results that:

- (1) As the Z stage moves up, the separation force increases gradually. After the cured layer is detached from the PDMS film, the separation force will drop rapidly from the peak value to 0;
- (2) Due to the flexibility of the PDMS film, the pulling-up force is rather small within a moving distance that is less than 200 $\mu\text{m}$ .
- (3) The peak force gets larger when the same mask image is exposed longer;
- (4) The peak force gets larger when a larger image area is projected;
- (5) The image shape has more complex effects on the peak force. In addition, their effects may interact with the exposure time and the projection area;

(6) With the coated PDMS film on the vat, the separation force is still considerably large (~100 oz or 27.8 N for an image area of 625mm<sup>2</sup> with 1 second exposure).

## 5.2 Separation Force Study based on the Two-way Movement Design

To verify the proposed two-way movement design, a set of experiments were conducted based on the setup as shown in Figure 6a. The same set of mask patterns were used in building test layers. The same exposure time and layer thickness were used (1 second and 0.2mm respectively). The building process as shown in Figure 5 was first used in building a set of layers. In the tests, the tank was translated in the X axis by 20mm. The moving speed is set at 25mm/sec. After the layers have been built, the pulling-up forces in the Z axis during building the next layer were recorded. However, instead of curing a new layer as shown in Step 3, the part is moved up slowly at 0.6mm/sec for 2.5mm. The measured forces of a sensor in the Z axis during the aforementioned three steps are shown in Figure 8. In each figure the curves record the test results based on a sampling resolution of 80 milliseconds.

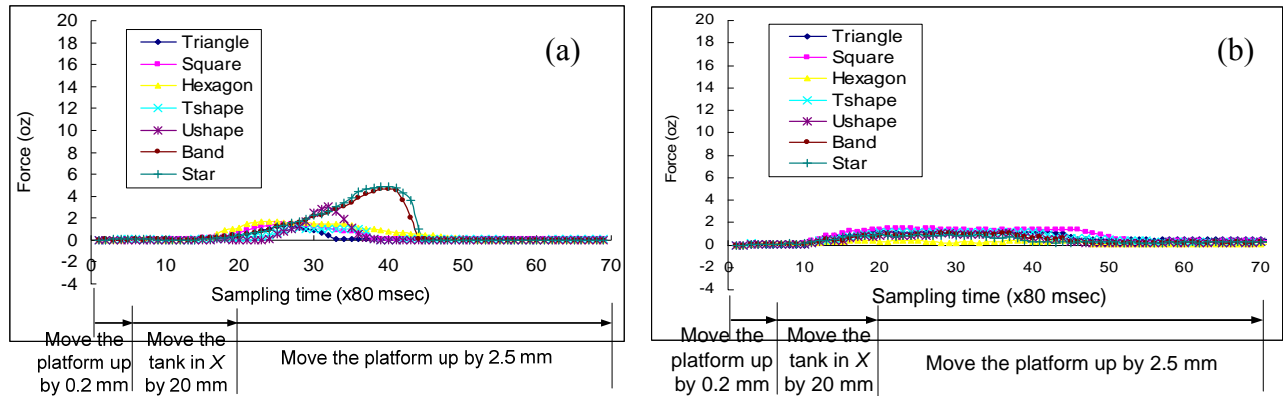


**Figure 8: Pulling-up forces of a cured layer based on the two-way movement design in different settings: (a)  $T=1\text{sec}$ , area = 625 mm<sup>2</sup>; (b)  $T=1\text{sec}$ , area = 156 mm<sup>2</sup>.**

The figures show that the force in the Z direction is rather small when the platform is moved up by 0.2mm. During the remaining two steps (i.e. sliding on the PDMS film and the platform pulling-up), the peak separation forces are also relatively small (around 2-6 oz or 0.56-1.67 N). Such measured forces are only 3-4% of the related ones as shown in Figure 7. Hence the two-way movement design can effectively reduce the large separation force in the bottom-up projection system.

## 5.3 Shearing Force Study in the X Axis

In the two-way movement design, cured layers can easily slide on the PDMS surface. The FlexiForce sensors were used in a modified setup to measure the shearing force in the X direction. However, no meaningful readouts were recorded from the sensors. To quantitatively estimate the value of the shearing force in the X axis, a set of square rods with different sizes were built using the two-way movement design. The built rods shown in Figure 9 are 10mm tall. The minimum cross section size is 0.4×0.4mm. Note that we also successfully built rods with even smaller sizes. However, the rods were so fragile that they lost the mechanical strength to sustain themselves when the part was taken out of the resin vat and washed in isopropyl alcohol.

Nevertheless, for a rod with a size of 0.4×0.4mm, the maximum tangential force that can be added on it can be analytically estimated. As shown in Figure 4b, the testing rods in the experiment can be modeled as a cantilever beam. Suppose the

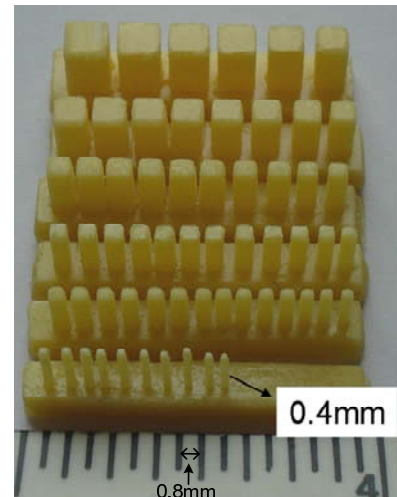


**Figure 9: Shearing force verification test.**

length of the beam is  $L$ , the size of the beam section is  $b \times b$ , the force in tangent direction is  $F$ . The maximum bending stress at the end can be calculated as:  $\sigma = Mc/I$ , where  $I$  is the section modulus,  $I = b^4/12$ , and  $c = b/2$ . Substituting these values for their variables, the resultant equation is  $\sigma = \frac{6FL}{b^3}$ .

Suppose the allowable bending stress is  $[\sigma]$  and the minimal beam section size is  $[b]$ . We will have the following equation:  $F \leq \frac{[\sigma][b]^3}{6L}$ . The material used in our tests has the following parameters:  $[\sigma] = 65\text{MPa}$ ,  $[b] = 0.4\text{mm}$ ,  $L = 10\text{mm}$ . According to the equation, the upper bound of the tangential force is only 0.07N or 0.25oz. Compared with the separation force in the  $Z$  direction, the shearing force in the  $X$  direction is rather small.

## 6 A FAST MACRO-SCALE MIP-SL PROCESS AND ITS BUILDING SPEED ANALYSIS

The two-way movement design enables the quick spreading of liquid resin into a uniform thin layer. In addition, the DMD-based digital mask projection enables the fast curing of the spread liquid resin into a desired solid layer. Consequently, for a given 3D CAD model, a fast MIP-SL process can fabricate a physical object within a short building time. The curing characteristics and the two-way movement settings of the developed macro-scale MIP-SL process are presented as follows. A detailed analysis of its building time is also discussed.

### 6.1 Curing Characteristics

There are two types of photopolymer systems, acrylate chemistry and cationic photopolymerization, in the SLA process [16]. Acrylate chemistry polymerizes via a free-radical mechanism while cationic photopolymerization undergoes ring-opening reactions in the presence of cationic photoinitiators. The monomer propagation for cationic reactions requires relatively higher activation energy. Consequently, the photospeed of acrylate-based photopolymers is higher due to the lower activation energy for free-radical reactions. Considering the photospeed difference, we selected the photopolymer resins based on acrylate chemistry for the developed fast MIP-SL process. As shown in Section 6, our projection system can cure a layer within a short exposure time (<500 milliseconds). Such a fast curing time contributes to the desired fast MIP-SL process for building 3D objects in minutes.

After an image is exposed for a certain time ( $T_{projection}$ ), a waiting time,  $T_{wait\_projection}$ , is required before the layer can be moved up for one layer thickness (i.e. Step 1 in Figure 5). Such a waiting time is critical in order for the acrylate resin to complete the solidification process and gain sufficient strength for the  $Z$  movement. Otherwise, the building process may fail. The waiting time is dependent on the resin's curing property. Due to the fast photospeed of the acrylate resins, the waiting time in our system is short (~300 milliseconds in our tests).

### 6.2 Two-way Movement Settings

In the two-way movement design, the cured part is first moved up for one layer in the  $Z$  axis and the tank is then translated in the  $X$  axis for a certain distance. The two linear movements have different accuracy and speed requirements.

(1) The  $Z$  movement needs to be accurate since it will determine the layer thickness of the next layer. The  $Z$  stage also needs to have a resolution that is much smaller than a layer thickness. Accordingly, to ensure the desired accuracy and resolution, we set small acceleration and velocity values in the  $Z$  movement. The slow movement of the cured part also enables the PDMS film to fully elastically deform for a small attaching force. However, the movement time in the  $Z$  axis ( $T_Z$ ) is still reasonably short (~0.4 second in our tests) since only a small moving distance is required (e.g. 50 or 100  $\mu\text{m}$ ).

(2) The tank needs to be moved in the  $X$  axis for a certain distance to release the elastic deformation of the PDMS film. The  $X$  moving distance is related to the shape and size of the cured layer, and less than the extent size of the cured layer in the  $X$  axis. Since the relative position of the platform and the

projection system will not change during the  $X$  movement, the accuracy and resolution requirements on the  $X$  movement are not as high as those on the  $Z$  movement. Hence a much larger acceleration and velocity can be applied in the  $X$  movement to reduce the movement time in the  $X$  axis ( $T_X$ ).

In our testbed, we used a  $Z$  linear stage with a thread of 0.5mm/round, and a  $X$  linear stage with a thread of 25.4mm/round. The moving time for different displacement distances in our prototyping system was calibrated for both linear stages. After the  $X$  movement, another waiting time,  $T_{wait\_X}$ , is required in order for the flowing liquid resin to settle. Otherwise, the building process may fail. The waiting time caused by the  $X$  motions is related to the movement distance and the moving speed. Due to the small gap between the cured part and the PDMS film, the required waiting time is typically short (~100 milliseconds). After the waiting time of  $T_{wait\_X}$ , the liquid resin forms a uniform thin layer, which is ready for the next layer to be built. The process can then be repeated after the related mask image is exposed.

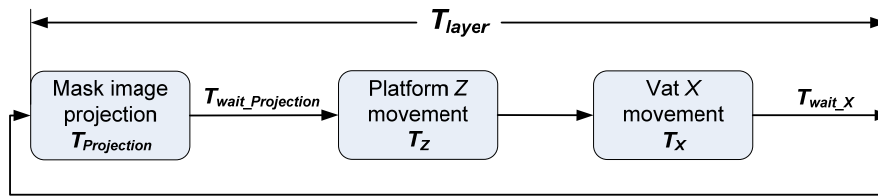


**Figure 10: The building time of a layer in the two-way movement based MIP-SL process.**

### 6.3 The Building Time of a Layer

As shown in Figure 10, the building time of each layer is thus the sum of all the aforementioned steps:

$$T_{Layer} = T_{Projection} + T_{wait\_Projection} + T_Z + T_X + T_{wait\_X}.$$

The first two items,  $T_{Projection}$  and  $T_{wait\_Projection}$ , are related to the curing characteristics of the photopolymer resins used in the MIP-SL process. The photopolymer resins based on acrylate chemistry can be quickly cured. A stronger light source used in the projection system can further reduce the projection time  $T_{Projection}$ .

The other three items,  $T_Z$ ,  $T_X$ , and  $T_{wait\_X}$ , are related to the two-way movement design.  $T_Z$  is related to the layer thickness and the moving velocity in the  $Z$  axis.  $T_X$  is related to the size of the cured layer and the moving velocity in the  $X$  axis. A linear stage with a higher speed can be used to further reduce the movement time  $T_X$ .  $T_{wait\_X}$  is determined by the gap distance between the PDMS and the cured layer, the moving velocity of the tank, the shape of the cured layer, and the flow properties of the liquid resin. For a typical layer thickness that is usually small,  $T_{wait\_X}$  is reasonably short (~100 millisecond in our tests).

Note that the projection time  $T_{Projection}$  for the first few layers is much longer (e.g. 3-4 seconds) to ensure the initial layers can be strongly bonded to the build platform, For all the other layers, the total building time of a layer is usually short (a few seconds in our tests). Hence a fast fabrication speed can be achieved in the developed process (e.g. building 3mm height per minute).

## 7 EXPERIMENTAL SETUP

### 7.1 Hardware System

A prototype system has been built to verify the developed process. The hardware setup of the fast MIP-SL system is shown in Figure 11. In the designed system an off-the-shelf projector (*CASIO XJ-S36*) was used. The optical lenses of the projector were modified to reduce the projection distance. Various projection settings including focus, key stone rectification, brightness and contrast were adjusted to achieve a sharp projection image on the designed projection plane. The DMD resolution in our system is 1024×768 and the envelope size is set at 48×36 mm. A precise linear stage from Aerotech Inc (Pittsburgh, PA) is used as the elevator for driving the platform in the  $Z$  axis. A fast linear stage from Servo Systems Co. (Montville, NJ) is used to drive the tanks back and force in the  $X$  axis. A high performance 4-axis motion control board with 28 Bi-directional I/O pins from Dynamotion Inc. (Calabasas, CA) is used for

driving the linear stages. A flat and clear glass Petri dish is used as resin tank. A PDMS film (Sylgard 184, Dow Corning) is coated on the glass dish.

## 7.2 Software System

A mask planning testbed has been developed using the C++ language with Microsoft Visual C++ compiler. The testbed integrates the geometry slicing and the motion controlling. It also synchronizes the image projection with the  $X$  and  $Z$  movements. The graphical user interface (GUI) of the developed software system and the flowchart of the fast MIP-SL process are shown in Figure 12.

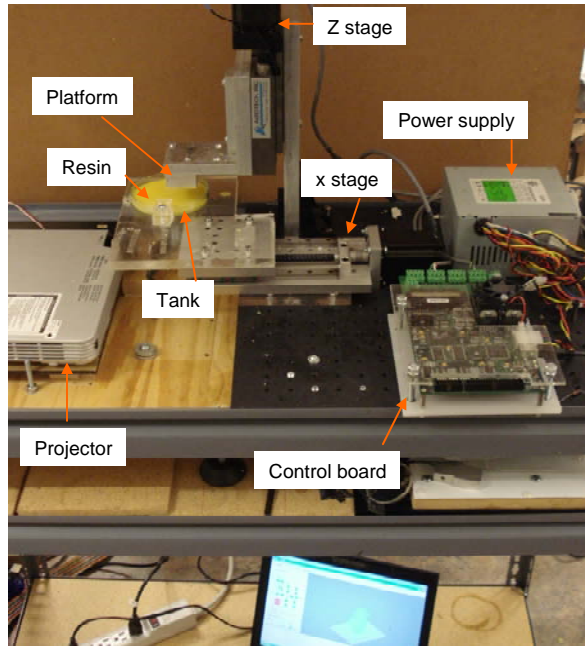


**Figure 11: The prototype hardware system for the fast MIP-SL process.**

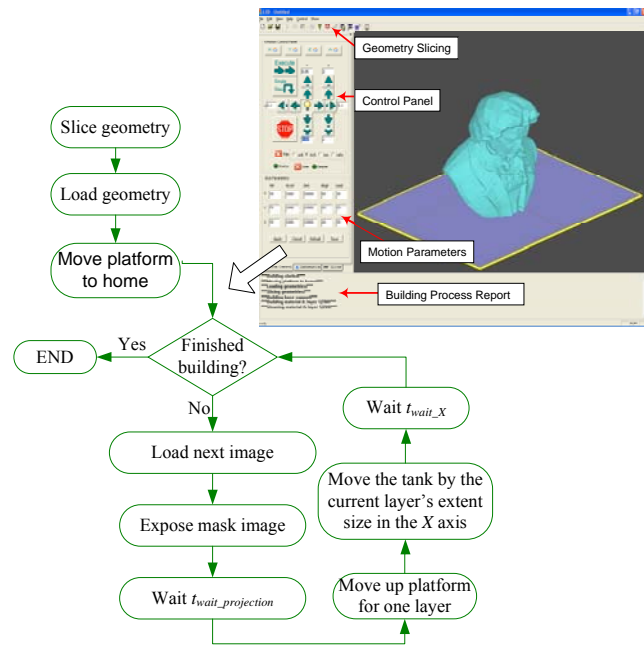


**Figure 12: Flow chart of the fast MIP-SL system and related software system.**

## 7.3 Materials

Perfactory™ SI500 (yellow) and Acryl R5 (red) from EnvisionTec Inc. (Ferndale, MI), were used in testing the developed fast MIP-SL process. Both resins belong to Acrylate. For curing depths of 0.05mm and 0.1mm, the exposure times for SI500 based on our projection system are set at 0.3 sec and 0.45 sec, respectively. The exposure times for Acryl R5 are set at 0.4 sec and 0.55 sec for curing depths of 0.05mm and 0.1mm, respectively.

## 8 EXPERIMENTAL RESULTS AND DISCUSSION

Tests have been performed to verify the building speed of the developed prototyping system. The results of the designed tests have demonstrated that the presented MIP-SL process can build 3D models in minutes instead of hours.

### 8.1 Test Results of Macro-scale MIP-SL

A set of CAD models with different complexity were used in our tests. The screenshots of six input CAD models are shown in Figure 13.a-18.a. The related STL files have triangle numbers ranging from several hundreds to 1.2 million (refer to Table 1).

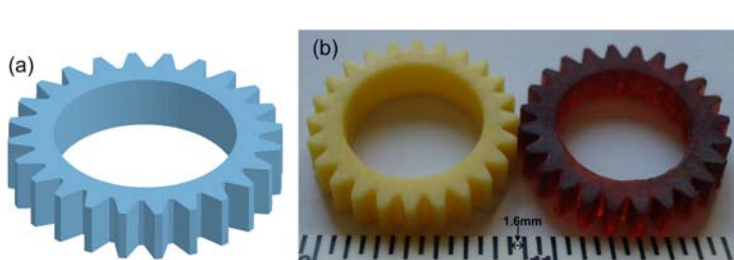
Two different layer thicknesses commonly used in the MIP-SL process were tested. A 50 $\mu$ m layer thickness was used in the fabrication of a gear model. The mask image projection time was 0.35 second for each layer except the base. The projection waiting time was set at 0.1 second. For all the other models, a 100 $\mu$ m layer thickness was used in their building processes. Due to the larger layer thickness, a longer

image exposure and projection waiting times were used (0.45 and 0.3 second respectively in the tests). Accordingly the Z movement will also take a longer time for a larger layer thickness. In the tests, the movement time in the Z axis ( $T_z$ ) is 0.32 and 0.42 second for the layer thickness of 50 $\mu$ m and 100 $\mu$ m, respectively.

The required moving distance in the X axis is related to the size and shape of the cured layer. For a layer with a big cross-section area (e.g. the models of a head and a statue), the X translation distance is set to a value that is close to the X extent size. Due to the large movement, the X waiting time was also set longer. In comparison, for a layer with a small cross-sectional area (e.g. the models of a hearing aid shell and the top portion of a brush), the X translation distance can be much smaller than the extent size of the layer in the X axis. However, due to the fast moving speed in the X axis, the differences on  $T_x$  are usually small (less than 1 second as shown in Table 1).

Two types of resins, SI500 and Acryl R5, were tested. Their curing characteristics are slightly different. For the same layer thickness, the curing of Acryl R5 takes  $\sim$ 0.1 second longer than that of SI500. The viscosities of the two resins are also slightly different. However, the same settings can be used in the two-way movement design based on the two resins.

Figure 12-17 show the built objects based on the developed fast MIP-SL process. The quality of the built objects was examined to be satisfactory. Both surface finish and dimension were analyzed to be acceptable. In our prototyping system, the nominal size of a pixel is 47 $\mu$ m. The fine image resolution enables the meso-scale features (i.e. in the range of 0.1-1 mm) to be well captured in the built physical objects, e.g. the lip of the human head, the cloth folds in the Beethoven statue, and the dentures in the teeth model.



**Figure 13: A test of a gear: (a) CAD model; (b) built objects in two liquid resins.**

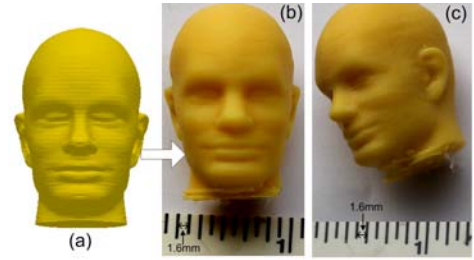


**Figure 14: A test of a head: (a) CAD model; (b-c) two views of the built object.**



**Figure 15: A test of a statue: (a) CAD model; (b-e) two views of the built objects in two resins.**

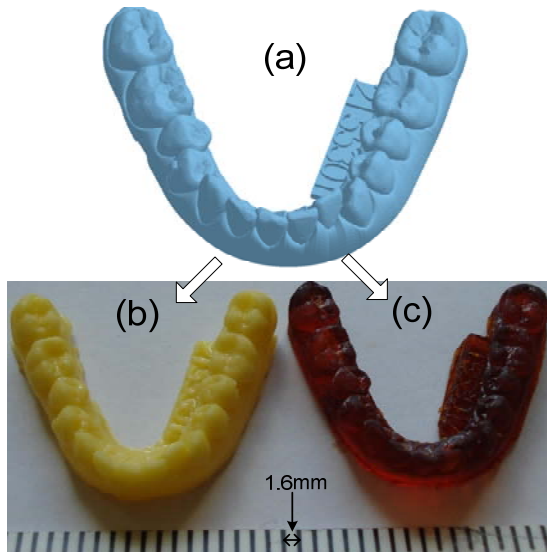


**Figure 16: A test of teeth: (a) CAD model; (b-c) built objects in two liquid resins.**

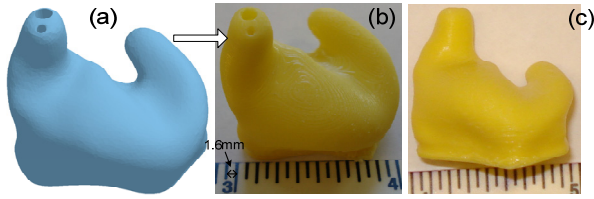


**Figure 17: A test of a hearing aid shell: (a) CAD model; (b-c) two views of the built object.**

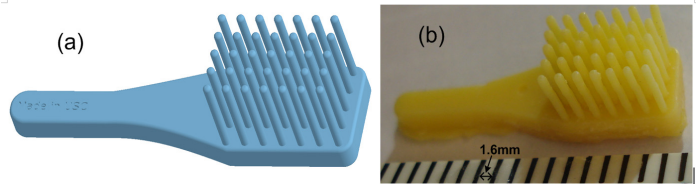


**Figure 18: A test of a brush: (a) CAD model; (b) built object.**

**Table 1: Building time statistics**

Model	Gear	Head	Statue	Teeth	Shell	Brush
Figure #	Fig.12	Fig.13	Fig.14	Fig.15	Fig.16	Fig.17
Tri #	660	24190	5204	133806	32762	1259246
Size <sub>x</sub> (mm)	25.4	25	17.7	24	24	7.6
Thickness (mm)	0.05	0.1	0.1	0.1	0.1	0.1
T <sub>projection</sub> (sec)	0.35 (0.4)*	0.45	0.45 (0.55)*	0.45 (0.55)*	0.45	0.45
T <sub>wait projection</sub> (sec)	0.1	0.3	0.3	0.3	0.3	0.3
T <sub>Z</sub> (sec)	0.32	0.42	0.42	0.42	0.42	0.42
Move <sub>x</sub> (mm)	7.6	25	12.7	2.5	2.5	6.35 (1.3) <sup>+</sup>
T <sub>X</sub> (sec)	0.58	1.1	0.67	0.46	0.46	0.56 (0.39) <sup>+</sup>
T <sub>X wait</sub> (sec)	0.05	0.1	0.1	0.05	0.05	0.05
T <sub>Layer</sub> (sec)	1.4 (1.45)*	2.37	1.94 (2.04)*	1.68 (1.78)*	1.68	1.78 (1.61) <sup>+</sup>
Height <sub>Z</sub> (mm)	4.93	28.5	30.5	7.3	22.3	8.3
Layer #	98	285	305	73	223	83
T <sub>total building</sub> (min)	2.31 (2.39)*	11.26	9.86 (10.4)*	2.04 (2.17)*	6.24	2.25

\* The projection and waiting time for R5 resin; others are for SI500.

<sup>+</sup> Different X moving distances were used in building the bottom (1<sup>st</sup> -19<sup>th</sup> layers) and the top (20<sup>th</sup> -83<sup>th</sup> layers) portions of the brush.

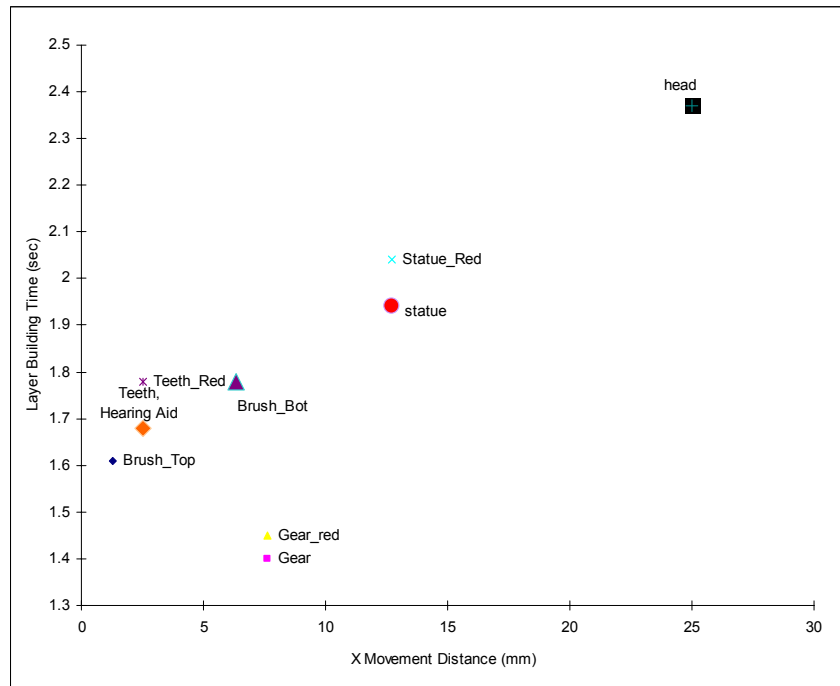


**Figure 19: Layer building time of the test cases.**

All the models shown in Figure 13-18 were built within 12 minutes using our prototyping system. The models with less than 100 layers (e.g. the gear, the teeth, and the brush) only require 2-3 minutes to be built. A statistic of the building time is given in Table 1.

A much larger exposure time (e.g. 4-5 seconds) was required for the first few layers in order to build a base. Consequently the built objects and the build platform can be well bonded. For all other layers, as shown in Figure 19, the building time of a layer ( $T_{Layer}$ ) in our MIP-SL process is only 1.4-2.5 seconds. The variation on  $T_{Layer}$  is mainly due to different layer thicknesses and the  $X$  moving distances. For an average of 2 seconds per layer and a layer thickness of 0.1mm, the building speed of the developed MIP-SL process is  $\sim 3$ mm per minute, or 180mm per hour. To the best of our knowledge, such a MIP-SL process is one of the fastest layer-based additive manufacturing processes that have been developed. A video of building the gear model as shown in Figure 13.a can be found in [17].

## 8.2 Test Results of Micro-scale MIP-SL

As discussed in Section 3, the recoating approach of moving the platform up-down in the  $Z$  direction is more appropriate for features that are small. Accordingly, we have developed a micro-scale MIP-SL prototyping system based on such an approach. The projection area is set at  $12.7 \times 8$  mm. Various tests have been performed to verify the capability of micro-scale fabrications based on the recoating approach. Two of the test cases are shown in Figures 20 and 21. Figure 20c and 21c show the microscopic images of gear teeth and curved shell with desired thickness ( $\sim 80\mu\text{m}$ ). The support rods as shown in Figure 21b have a diameter around  $60\mu\text{m}$ .

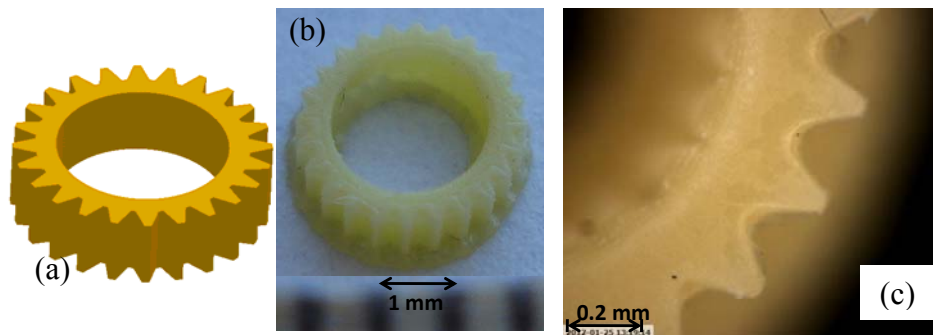


Figure 20: A micro gear: (a) CAD model; (b) Built part; (c) Microscopic picture of the gear teeth.

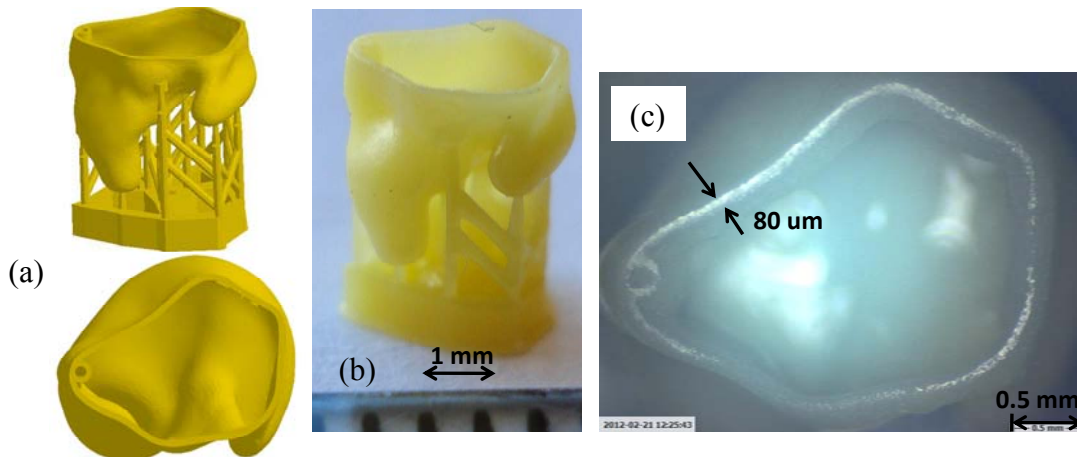


Figure 21: A micro-scale hearing-aid: (a) CAD model of hearing-aid: (a) CAD model with supports for building job; (b) built part; (c) Micro scope picture of the top view of the built part.

## 9 CONCLUSIONS

A novel mask-image-projection-based stereolithography process has been presented for fabricating 3D objects with fast building speed. The proposed approach is based on projecting mask images bottom-up on a PDMS coated glass substrate. A new two-way movement design has been presented for quickly spreading liquid resin into uniform thin layers for macro-scale parts. Such a design can significantly reduce the separation force between cured layers and the resin tank. Experimental results verified that the separation force as well as the sliding force are relatively small during the two-way movement process. The motions related to the two-way movement design can also be performed quickly. The MIP-SL process developed based on such a recoating approach can achieve high fabrication speed for input CAD models. The experimental results demonstrate that the newly developed MIP-SL process can successfully fabricate 3D objects with satisfactory quality in a short time (usually in minutes).

Some future work to further improve the building speed of the developed MIP-SL process includes: (1) investigating the settings of  $T_x$  and  $T_{wait\_X}$  based on given layers for the best performance; (2) testing faster moving speeds in the X and Z axes; and (3) testing the two-way movement design in prototyping systems with larger XY extent sizes.

## REFERENCES

- [1] Bourell, D., M. Leu, and D. Rosen (2009). "NSF workshop - roadmap for Additive Manufacturing: identifying the future of freeform processing." Washington, D.C., March 30-31, 2009.
- [2] Chatwin C., M. Farsari, S. Huang, M. Heywood, P. Birch, R. Young, J. Richardson (1998). "UV micro-stereolithography system that uses spatial light modulator technology," *Applied Optics*, Vol. 37, pp.7514-22.
- [3] Bertsch, A., P. Bernhard, C. Vogt, P. Renaud (2000). "Rapid prototyping of small size objects." *Rapid Prototyping Journal*, Vol. 6, Number 4, pp. 259-266.
- [4] Stampfl, J., H. Fouad, S. Seidler, R. Liska, F. Schwager, A. Woesz, P. Fratzl (2004). Fabrication and moulding of cellular materials by rapid prototyping. *Int. J. Materials and Product Technology*, Vol. 21, No. 4, pp 285-296.
- [5] Sun C., N. Fang, D. Wu, X. Zhang (2005). Projection micro-stereolithography using digital micro-mirror dynamic mask. *Sensors and Actuators A*. Vol. 121, pp. 113-120.
- [6] Lu, Y., G. Mapili, G. Suhali, S.C. Chen, K. Roy (2006). A digital micro-mirror device (DMD)-based system for the microfabrication of complex, spatially patterned tissue engineering scaffolds, *Journal of Biomedical Materials Research A*, Vol. 77A (2), pp. 396-405.
- [7] Limaye, A, D. W. Rosen (2007). Process planning method for mask projection micro-stereolithography, *Rapid Prototyping Journal*, Vol. 13, No. 2, pp. 76-84.
- [8] Choi, J., R. B. Wicker, S. Cho, C. Ha, and S. Lee (2009). Cure depth control for complex 3D microstructure fabrication in dynamic mask projection microstereolithography, *Rapid Prototyping Journal*, Vol. 15 (1), pp. 59-70.
- [9] EnvisionTEC: <http://www.envisiontec.de>, visited on Sept/1/2011.
- [10] V-Flash desktop modeler: <http://www.modelin3d.com>, visited on Sept/1/2011.
- [11] Chen. Y., Zhou, C., and Lao, J. (2011). "A layerless additive manufacturing process based on CNC accumulation." *Rapid Prototyping Journal*, Vol. 17, No. 3, pp. 218-227.
- [12] Huang, Y.M., Jiang, C.P. (2005). "On-line force monitoring of platform ascending rapid prototyping system", *Journal of Materials Processing Technology*, Vol. 159 pp.257-64.
- [13] SLP-4000 Solid Laser Diode Plotter, Product Brochure (1997), Denken Corporation, Japan.
- [14] Dendukuri, D., Pregibon, D. C., Collins, J., Hatton, T. A., and Doyle, P. S. (2006). "Continuous-flow lithography for high-throughput microparticle synthesis". *Nature Mater.*, Vol. 5, pp. 365–369.

- [15] Zhou, C., Y. Chen. Y., Z. Yang, and B, Khoshnevis (2011). "Development of multi-material mask-image-projection-based stereolithography for the fabrication of digital materials." Proceedings of Annual Solid Freeform Fabrication Symposium, Austin, TX.
- [16] Jacobs, P. F. (1995). *Stereolithography and Other RP&M Technologies: From Rapid Prototyping to Rapid Tooling*. Society of Manufacturing Engineering.
- [17] Youtube - Fast MIP-SL process demo: <http://www.youtube.com/watch?v=M4jQuXZ9vqI>, visited on Aug/5/2012.